A Concurrent 2.2/3.9-GHz Dual-Band GaN Power Amplifier

Philip Zurek, Tommaso Cappello, and Zoya Popović

Department of Electrical, Computer, and Energy Engineering
University of Colorado, Boulder, Colorado, 80309, USA

***Abstract*— This paper presents an efficient concurrent dual-band 2.2/3.9 GHz hybrid power amplifier, designed with a 0.25-μm Qorvo 15 W GaN HEMT. In non-concurrent CW mode, peak PAEs of 74.4% and 57.7% are measured at the two frequencies, respectively, with 41.7 and 41.2 dBm output power and 13.9 and 9.37 dB gain at 3 and 1 dB compression. When two concurrent 10-MHz 6-dB PAPR multitone signals are amplified, the average PAE reaches 55%, with ACLRs of -42.5 and -43.3 dBc in the two bands obtained after digital pre-distortion.**

I. Introduction

There has been a continuing trend to decrease the number of power amplifiers (PAs) in a multi-band transmitter in order to reduce size, while the number of bands continues to increase. Multi-band, e.g. [1]–[3] as well as tunable, e.g. [1], [4], [5] PAs have been demonstrated to address this need. In these PAs, the active device is matched at two or more fundamental frequencies and their harmonics, using typical CW PA performance enhancement techniques. The case of several simultaneous modulated signals is considered in [6], [7]. Here we present a more detailed study of efficient amplifier design and behavior in concurrent mode.

Many of the efficiency improvement techniques developed for CW PAs, such as reduced conduction angle [6], harmonic terminations [2], [7], and using the transistor as a switch have been applied to dual-band PAs. In some tunable PAs, varactors are used in the matching networks, requiring an additional reverse-bias supply [4]. In non-concurrent mode, switches can be used to toggle between two different single-frequency PAs, increasing performance at the expense of size and complexity [5].

Harmonic terminations in multi-band PAs require simultaneous matching to many impedance values. In [2] a 7-element LC ladder network is used to terminate the first two harmonics of a class-F dual-band PA. These are then transformed to microstrip lines to be realized as a MMIC. Composite right/left-handed transmission lines are used by [7] to similarly terminate the first two harmonics of a class-F dual-band PA with two such transmission lines, simultaneously at two frequencies.

In this paper, we report on the design and characterization of a dual-band PA for concurrent signal transmission at 2.2 and 3.9 GHz carrier frequencies, with an emphasis on efficiency and linearity, Fig. 1. Table I compares results found in the literature and this work. A discussion of the design, implementation and characterization of the dual-band PA in non-concurrent and concurrent operation using multi-tone 10-MHz signals with a peak-to-average power ratio (PAPR) of 6 dB is presented. Linearity is accomplished with digital pre-distortion (DPD) designed by characterizing the cross-modulation between the two concurrent band signals.

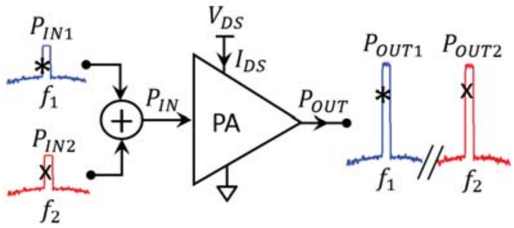

Fig. 1. Concept block-diagram of the dual-band PA for concurrent signal amplification. Signals modulated onto two broadly separated carriers at $f_1 = 2.2$ GHz and $f_2 = 3.9$ GHz are concurrently amplified with high efficiency with a single load.

TABLE I. Summary of Dual-Band PA Performance

Ref.	Freq. (GHz)	PAE (%)	P_{OUT} (dBm)	Gain (dB)
[8]	1.9/2.6	62.9/56.2	44.5/44	15/12
[2]	0.8/1.85	69.4/68.9	42.7/41.8	19.8/16.7
[3]	1.8/2.4	60/58	41/40	12/11
[1]	5/12	58/51	28/26.7	12/10.3
[6]	1.7/2.14	78/77.1	40.5/39.8	12.5/11.8
[4]	0.68/1.84	61.3/52.7	41/41.9	11/10
[5]	1.8/2.3	60.1/56.5	40.9/39.8	12/8
[9]	3.5/5.5	40.4/39.9	36.7/37.1	9.7/6.4
This work	**2.2/3.9**	**74.4/57.7**	**41.7/41.2**	**13.9/9.37**

II. Dual-Band Power Amplifier

Simulated load-pull power-added efficiency (PAE) and P_{out} contours for the 0.25-μm 15 W Qorvo GaN HEMT device (T2G6001528-SG) at the fundamental frequencies of the two bands, Fig. 2, are used as a starting point for dual-band output matching network design. Target design load impedances of $Z_L(f_1) = 9.99 + j4.78\,\Omega$ and $Z_L(f_2) = 11.78 - j4.51\,\Omega$ are chosen as a trade-off between maximal PAE and P_{OUT} values (marked in plot), resulting in predicted PAE=70/58 % and P_{OUT}=41.5/39.2 dBm at the lower/upper band. A similar procedure is used from simulated source pull contours to determine target source impedances. Note the sensitivity to impedance of the PAE contours, which are closely spaced for low impedance values, Fig. 2(b).

978-1-5386-5947-2/19/$31.00 ©2019 IEEE

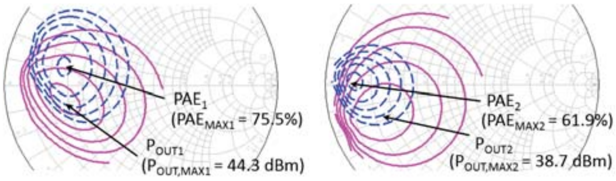

Fig. 2. Fundamental load-pull of the Qorvo GaN 15-W GaN-on-SiC HEMT at 2.1 GHz (left) and 3.7 GHz (right). PAE contours (dashed blue lines) are shown in steps of 5 percentage points whereas P_{OUT} contours (solid red lines) are indicated in steps of 1 dB.

Due to the bilateral nature of the device, each matching network requires at least eight tuning variables to achieve the four complex impedance points determined from the load and source-pull simulations. Initial simulations show that the topology of [2] can present these impedances to the device. Because of the close load-pull contour spacing, lumped component tolerance values could significantly affect matching performance. Bias lines are designed with a 6 nH inductor with Q = 154 and SFR = 6 GHz placed along each stub of the matching network to ensure a high RF impedance. Looking into the gate bias network, simulations give $|Z_{GB}| = 176/1350\,\Omega > |Z_{IMN}| = 9.72/188\,\Omega$ at the two carrier frequencies. Similarly, $|Z_{DB}| = 130/494\,\Omega > |Z_{OMN}| = 97.5/190\,\Omega$, refering to Fig. 3. A larger inductance has a lower SRF and affects the higher band. The inductor in combination with the rest of the bias line is designed as a band-reject filter, with center frequency between the two design frequencies, to present an approximate open circuit.

Considering both small and large-signal performance, a dual-band PA on a 30 mil Rogers 4350B substrate with $\epsilon_r = 3.33$ is designed to operate efficiently at 2.1 and 3.7 GHz. Because the device has less gain at higher frequencies, the PA is designed to operate 1 dB in compression at the upper frequency to maintain an acceptable amount of gain. At the lower frequency, the devices operates 3 dB in compression to maximize efficiency.

The final simulated impedances at the two carrier frequencies are $Z_L(f_1) = 14.61 + j6.45\,\Omega$ and $Z_L(f_2) = 10.95 - j7.72\,\Omega$, with second harmonic impedances of $Z_L(2f_1) = 3.09 + j17.41\,\Omega$ and $Z_L(2f_2) = 37.06 - j9.00\,\Omega$. According to [10], PA efficiency increases as the second harmonic moves away from the center of the Smith chart towards a short or open. The second harmonic impedance at f_1 =2.1 GHz lies in the region of the Smith chart 18 points above nominal efficiency for a Class-A PA, near the upper limit, while that of f_2 =3.7 GHz lies 6 points above, chosen to maintain appropriate output power. Stability is verified with linear and nonlinear models of the HEMT over multiple gate bias voltages. A stability network consisting of a parallel 18-Ω resistor and 4.7 pF capacitor is included in the gate circuit. The complete fabricated circuit is shown in Fig. 3.

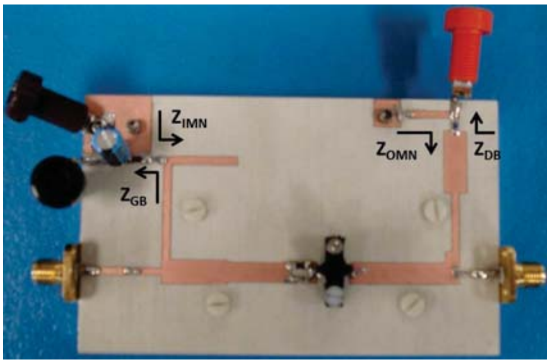

Fig. 3. Photograph of hybrid dual-band PA, measuring 106 x 114 mm.

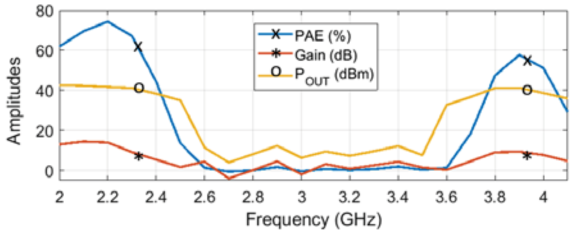

Fig. 4. Measured CW performance of the PA over frequency. Peak efficiencies are observed at 2.2 and 3.9 GHz.

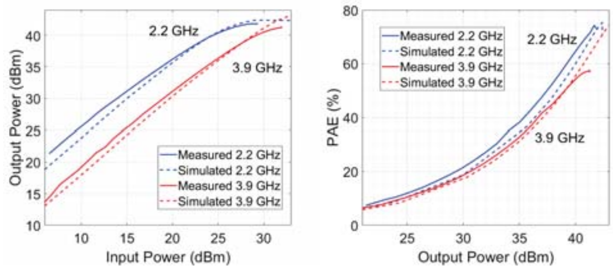

(a) (b)

Fig. 5. Static characterization of the dual-band PA in terms of (a) output power and (b) PAE. Simulated (dashed lines) and measured values (solid lines) show good agreement.

III. CW Dual-Band PA Characterization

The PA is first characterized in non-concurrent CW operation. The device is biased at 28 V and 19 mA for a deep-AB class of operation. The maximal PAE frequency points are shifted 4.8 % from 2.1 to 2.2 GHz, and 5.4 % from 3.7 to 3.9 GHz, seen in the measured broadband frequency response in Fig. 4. This shift can be attributed to the sensitivity of the PAE load-pull contours to fabrication tolerances. Plots of simulated and measured saturated gain, P_{OUT}, and PAE at the two peak-PAE frequencies are shown in Fig. 5. The drop in PAE at 3.9 GHz can be attributed to the gain discrepancy near compression between simulations and measurements due to limited output power of the driver in the upper band.

IV. Tests with Modulated Signals

The PA is next evaluated with two different multitone signals with 10-MHz bandwidth and 6-dB PAPR. Two synchronized National Instruments VSTs (PXIe-5646 and PXIe-5645), with bandwidths of 200 and 80 MHz, generate two broadly spaced signals at 2.2 and 3.9 GHz, with PEP of 28 and 32 dBm at the PA input, respectively. These two signals are summed using a broadband combiner to generate an appropriate multi-tone signal, detailed later. A linear wideband driver is used to increase signal power to drive the PA, without introducing significant intermodulation products. The driver output is attenuated and split with another broadband divider to feed the two VSTs. Pulsed characterization is performed with the PA biased at $V_{DS,Q} = 28\,\mathrm{V}$ and $I_{DS,Q} = 19\,\mathrm{mA}$.

Figs. 7(a)-8(a) show the narrowband gain of the PA. An AM gaussian pulse of $10\,\mu$s duration and $100\,\mu$s repetition period is used to sweep the input and output powers of the PA in the lower band. Simultaneously, an AM rectangular pulse of variable amplitude is used as the input in the higher band in order to quantify the gain degradation due to concurrent operation, Fig.7(a). The pulse shape is then switched between the two bands, Fig.8(a). When the PA is operated in non-concurrent mode , the gain is maximized. Interestingly, the back-off gain of the upper band increases when a second signal is injected; this effect is most likely due to a higher bias current and thus transconductance, which is introduced by the concurrent signal.

Figs. 7(b)-8(b) highlight the gain dispersion of the PA when driven with two different, 10-MHz, 6-dB PAPR signals. Significant cross-modulation is manifested by widely scattered points, which are however confined in the boundaries obtained with the narrowband characterization of Figs. 7(a)-8(a). We verified experimentally that the PA characteristics are not sensitive to the phase difference between the two input signals but only to their amplitudes. This allows a bi-dimensional memory polynomial (2-D MP) model in which the output is only dependent on the amplitudes of the two input signals [11]. It is worth mentioning that when one of the two signals is disabled, the 2-D MP reduces to a well-known 1-D MP model. This corresponds to the case of non-concurrent gain from Figs. 7(a)-8(a) . We employ a 2-D MP model for predistortion with an indirect learning approach; a nonlinearity order of 7 and memory of order of 1 are selected for the DPD model.

Linearized gains of the dual-band PA are measured to be 10.2 dB and 8.0 dB at 2.2 and 3.9 GHz, respectively. Figs. 7(c)-8(c) show two concurrent output spectra for the two bands. As the input power of the concurrent signal is backed-off, we observe a more confined spectrum, likely due to better linearization at lower levels of cross-modulation. As shown in the insets of Figs. 7(c)-8(c), the PAE is maximized at the nominal input drive (i.e. $P_{IN1} = 28\,\mathrm{dBm}$ and $P_{IN2} = 32\,\mathrm{dBm}$) and peaks at 55% while the ACLR is -42.5/-43.3 dBc. We note that this high PAE value is mainly due to a lower PAPR of

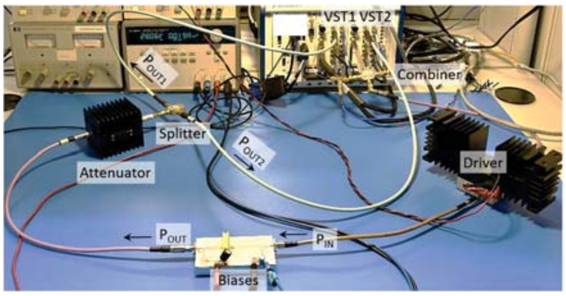

Fig. 6. Setup for the dynamic characterization of the dual-band PA in concurrent mode. Two VSTs are employed to generate two broadly-spaced concurrent signals which are combined and injected in the PA. The output of the PA is then splitted and sampled around the two carrier frequencies by the VSTs.

the resulting output signal (4.42 dB at the maximum input powers). As the opposite signal power is backed-off, an efficiency degradation is observed while ACLR improves, as seen in Fig. 9.

V. Conclusion

In summary, this paper discusses a design approach for a dual-band PA which results in best-of-class CW PAE of 74/57% at 2.2/3.9 GHz. The PA is characterized in non-concurrent and concurrent modes over the two bands with 10-MHz, 6-dB PAPR multitone signals. The PA is tested at different average power levels in the two concurrent bands, showing the specific tradeoff between linearity and efficiency in concurrent mode. An average PAE efficiency of 55% and ACLRs as low as -42.5/-43.3 dBc in the two bands are demonstrated.

Acknowledgment

This work is supported in part under the Assistant Secretary of Defense (ASD) for Research and Engineering Contract No. FA8721-05-C-0002 and/or FA8702-15-D-0001. Any opinions, findings, conclusions or recommendations expressed in this material are those of the authors and do not necessarily reflect the views of the ASD. Simulation models utilized under the University License Program from Modelithics, Inc., Tampa, FL and Qorvo, Portland, Oregon. The authors thank National Instruments for generous gift and equipment support.

References

[1] G. Nikandish, E. Babakrpur, and A. Medi, "A harmonic termination technique for single- and multi-band high-efficiency class-f mmic power amplifiers," *IEEE Trans. Microw. Theory Techn.*, vol. 62, no. 5, pp. 1212–1220, May 2014.

[2] J. Shao, D. Poe, H. Ren, B. Arigong, M. Zhou, J. Ding, R. Zhou, H. S. Kim, and H. Zhang, "Dual-band microwave power amplifier design using gan transistors," in *2014 IEEE 57th Int. Midwest Symp. Circ. Syst. (MWSCAS)*, Aug 2014, pp. 559–562.

[3] E. Arabi, P. E. de Falco, J. Birchall, K. A. Morris, and M. Beach, "Design of a triple-band power amplifier using a genetic algorithm and the continuous mode method," in *2017 IEEE Topical Conf. RF/Microwave Power Ampl. Radio Wireless Appl. (PAWR)*, Jan 2017, pp. 48–51.

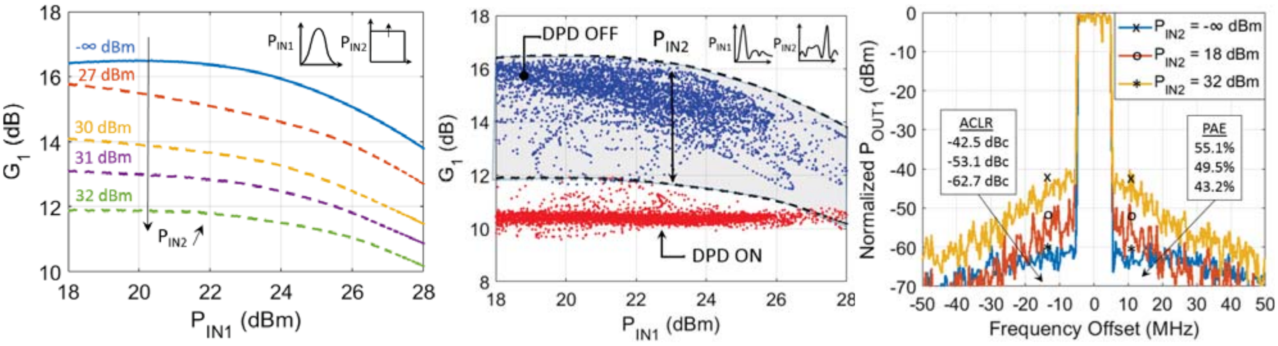

(a) (b) (c)

Fig. 7. Experimental variable-amplitude pulsed characterization of the lower band of the PA operated concurrently with a rectangular pulse at the upper band; (a) PA gain showing the degradation induced by a concurrent signal P_{IN2}. (b) Gain dispersion of the PA when fed with a modulated 10-MHz, 6-dB PAPR signal; DPD is however capable to recover the cross-modulation distortion. (c) Output spectra of the linearized dual-band PA in the 2.2 GHz band.

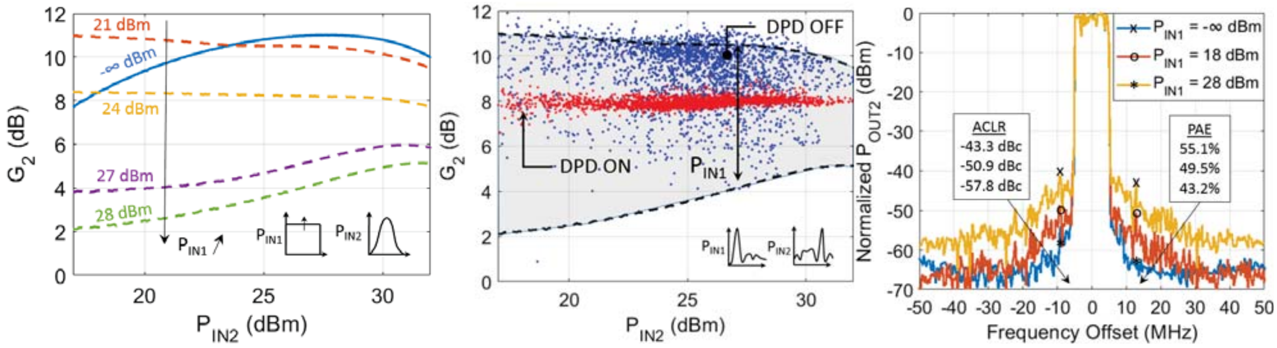

(a) (b) (c)

Fig. 8. Experimental variable-amplitude pulsed characterization of the lower band of the PA operated concurrently with a rectangular pulse at the upper band; (a) PA gain showing the degradation induced by a concurrent signal P_{IN2}. (b) Gain dispersion of the PA when fed with a modulated 10-MHz, 6-dB PAPR signal; DPD is however capable to recover the cross-modulation distortion. (c) Output spectra of the linearized dual-band PA in the 3.9 GHz band.

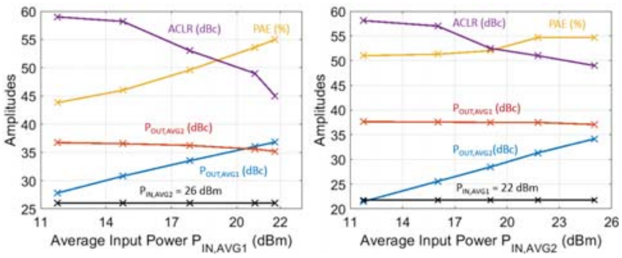

Fig. 9. Measured performance of the dual-band PA in concurrent mode at different input powers with modulated signals and DPD. The PA efficiency peaks at about 55% for the lower (left) and higher band (right) when driven with nominal input powers $P_{IN1} = 28$ dBm and $P_{IN2} = 32$ dBm. An opposite trend is observed for the ACLR metric.

[4] C. Sanchez-Perez, M. Ozen, C. M. Andersson, D. Kuylenstierna, N. Rorsman, and C. Fager, “Optimized design of a dual-band power amplifier with sic varactor-based dynamic load modulation,” *IEEE Trans. Microw. Theory Techn.*, vol. 63, no. 8, pp. 2579–2588, Aug 2015.

[5] R. Kalyan, K. Rawat, and S. K. Koul, “Design of reconfigurable concurrent dual-band power amplifiers using reconfigurable concurrent dual-band matching network,” in *2016 IEEE MTT-S Int. Wireless Symp. (IWS)*, March 2016, pp. 1–4.

[6] S.-K. Zhu, Q.-F. Cheng, H.-P. Fu, H.-F. Wu, and J.-G. Ma, “A highly efficient concurrent dual-band class-f power amplifier for applications at 1.7 and 2.14 ghz,” in *2015 IEEE MTT-S Int. Microw. Symp.*, May 2015, pp. 1–4.

[7] Q. F. Cheng, H. P. Fu, S. K. Zhu, and J. G. Ma, “Two-stage high-efficiency concurrent dual-band harmonic-tuned power amplifier,” *IEEE Trans. Microw. Theory Techn.*, vol. 64, no. 10, pp. 3232–3243, Oct 2016.

[8] X. Chen, W. Chen, G. Su, F. M. Ghannouchi, and Z. Feng, “A concurrent dual-band 1.9-2.6-ghz doherty power amplifier with intermodulation impedance tuning,” in *2014 IEEE MTT-S Int. Microw. Symp. (IMS2014)*, June 2014, pp. 1–4.

[9] T. Cappello, A. Duh, T. W. Barton, and Z. Popovic, “An efficient dual-band carrier-aggregation power amplifier with output diplexer,” *Submitted to IEEE Trans. Microw. Theory Techn.*, 2018.

[10] M. Roberg and Z. Popovic, “Analysis of high-efficiency power amplifiers with arbitrary output harmonic terminations,” *IEEE Transactions on Microwave Theory and Techniques*, vol. 59, no. 8, pp. 2037–2048, Aug 2011.

[11] S. A. Bassam, M. Helaoui, and F. M. Ghannouchi, “2-d digital predistortion (2-d-dpd) architecture for concurrent dual-band transmitters,” *IEEE Trans. Microw. Theory Techn.*, vol. 59, no. 10, pp. 2547–2553, Oct 2011.